

# Influence of Ventricular Pressure Drop on Mitral Annulus Dynamics Through the Process of Vortex Ring Formation

ARASH KHERADVAR<sup>1</sup> and MORTEZA GHARIB<sup>2</sup>

<sup>1</sup>Department of Mechanical Engineering, University of South Carolina, 300 Main Street, Columbia, SC 29208, USA; and  
<sup>2</sup>Cardiovascular and Biofluid Dynamics Laboratory, California Institute of Technology, 1200 E California Blvd., Pasadena, CA 91125, USA

(Received 23 January 2007; accepted 11 September 2007)

**Abstract**—Several studies have suggested that the mitral annulus displacement and velocity in early diastole can be used as indicators of diastolic performance. The peak velocity of the mitral annulus away from the LV apex during early diastole, which indicates the rate of longitudinal expansion of the LV, is reduced in patients with impaired diastolic relaxation. With the intention of relating the trans-mitral flow to mitral annulus plane dynamics, we measured mitral annulus recoil force for different valve sizes, while applying an exponential pressure drop in a simplified model of the ventricle. The temporal changes in diameter of the valve during rapid filling phase were also considered. The process of ventricular vortex formation was studied together with the measurement of mitral annulus recoil force within different pressure drop conditions. Matching the vorticity contour plots with the recoil force measurements resulted in the fact that the magnitude of recoil is maximal once the vortex ring is about to pinch off, regardless of the valve size or the characteristics of ventricular pressure drop. This study showed that the mitral annulus recoil is maximal once occurs at the vortex formation time ranging from 3.5 to 4.5. It was also shown that the presence of leaflets would dissipate the annulus recoil force.

**Keywords**—Vortex ring, Vortex formation time, Left ventricle, Diastole, Mitral annulus recoil.

## INTRODUCTION

Dynamics of mitral valve annulus during diastole is a topic that has received much attention recently given its important effects on valve performance in addition to its close association with diastolic heart failure (HF). The current literature strongly supports the dynamic motion of the mitral annulus during diastole on the basis of the extensive studies performed in both experimental animals and human subjects using roentgenogram marker

imaging,<sup>20,21</sup> sonomicrometry,<sup>22</sup> MR Imaging,<sup>36</sup> and echocardiography.<sup>45,46</sup> The annulus motion is relative to the ventricular apex and is a function of ventricular chamber shape, the trans-mitral flow, the papillary muscles and the chordate, respectively.

Several studies have suggested that the mitral annulus displacement<sup>1,38</sup> and velocity<sup>47,51,58</sup> in early diastole can be used as indicators of diastolic performance.<sup>14,15,25,32</sup> It has also been shown previously that during the development of HF, normal pattern of left ventricular (LV) filling would be altered due to the diastolic dysfunction.<sup>2,10,42,43</sup> This variation in trans-mitral flow would be reflected in diastolic motion of the mitral annulus measurable by Doppler tissue imaging (DTI).<sup>41</sup> The peak velocity of the mitral annulus away from the LV apex during early diastole ( $E_M$ )—which indicates the rate of longitudinal LV expansion—is reduced in patients with impaired diastolic relaxation.<sup>25</sup>

Several factors such as trans-mitral flow, ventricular compliance and papillary muscles can influence the mitral valve dynamics. The effect of trans-mitral flow can be analyzed through studying the characteristics of the trans-mitral vortex ring formed at early diastole.<sup>5,30,53</sup> Formation of a vortex ring due to the early diastolic flow was initially recognized by *in vitro* visualization of the trans-mitral flow<sup>4,48</sup> and subsequently confirmed by analyses based on color Doppler mapping<sup>34,56</sup> and MR Imaging.<sup>33,35</sup> The early trans-mitral flow is considered a rapidly starting jet that forms a vortex ring. The process of vortex ring formation is described by the vortex formation time which is a non-dimensional parameter<sup>18</sup>:

$$T^* = \frac{\bar{U}}{D} T_p \quad (1)$$

where  $\bar{U}$  is the mean velocity of the jet,  $T_p$  is the pulse duration, and  $D$  is the diameter of the nozzle. The importance of this parameter lies in the fact that by increasing it beyond a certain range (~3.5–4.5) for a

Address correspondence to Arash Kheradvar, Department of Mechanical Engineering, University of South Carolina, 300 Main Street, Columbia, SC 29208, USA. Electronic mail: arashkh@enr.sc.edu

starting jet, no additional energy or circulation enters the leading vortex ring, and the remaining fluid in the pulse ejects as a trailing jet.<sup>18</sup> A recent study<sup>17</sup> has suggested that the vortex formation time can be used as an additional index to differentiate the normal status from the diastolic dysfunction. This study has shown that the distribution of vortex formation time computed from the fully open mitral valve in healthy volunteers converges to a unique range of values between 3.5 and 5.0. Meanwhile, this index is notably lower in patients diagnosed with dilated cardiomyopathy (DCM).

Previously, computation of trans-mitral vortex formation time was mostly based on size of the fully open mitral valve,<sup>17</sup> not considering the temporal changes in effective valve opening diameter due to the leaflet kinematics. In the present study, we correlate the trans-mitral pressure drop in a simplified model of the left ventricle, with the mitral annulus recoil through the index of vortex formation time computed from the early diastolic flow profile, and the mitral valve's leaflets kinematics.

The objective was to understand the dynamics of mitral annulus and its pure correlation with trans-mitral flow by avoiding the effects of other parameters involved in the LV such as the muscle contraction, tissue deformation, and blood viscosity. In a normal ventricle, the mitral annulus motion is mainly a consequence of compliance effect and passive stiffness of myocardium. However, the compliant walls of the ventricle would affect generation of a vortex ring along with the trans-mitral jet, by dropping the LV pressure (suction effect) during diastole,<sup>53</sup> and would literally interact with the formed vortex.<sup>3</sup> As a result, we chose to generate vortex ring using an exponential pressure drop, mimicking the suction in the left ventricle<sup>57,62</sup> while carefully avoiding the influence of other factors.

## METHODS

The experimental setup was developed to imitate the trans-mitral flow during early diastole due to the rapid pressure drop in LV. In a normal heart, the mitral valve opens due to the ventricular pressure drop allowing the flow from atrium to ventricle. The ventricle expands and the valve moves in an opposite direction with respect to the flow. To be consistent with cardiac physiology, in the present study, the LV pressure drop in early diastole was forced to decay as an exponential function with a pressure-drop time constant ( $\tau$ )<sup>57</sup> in physiologic range<sup>13,16,44,61</sup> (2).

### *Experimental Setup Components*

The experimental setup was composed of two chambers partially filled with water; the nominal ven-

tricle was built as a Plexiglas chamber connected to a suction pump (VSI SPS3891, Vivitro Systems Inc.) to generate pressure drop, and the nominal atrium was a cylindrical tube sitting inside the ventricular chamber as shown in Fig. 1. Dimensions of the ventricular box were 13 cm (width) by 13 cm (depth) by 20 cm (height). However, only the lower 13 cm of the box was filled with fluid (Fig. 1). The diameter of the atrial tube was 7.5 cm. The base–apex distance was set to 9 cm similar to the LV base–apex distance according to medical literature.<sup>49,52</sup> The mitral annulus plane was replicated as a flat plate with a circular orifice for placement of a mitral bioprosthesis. Additionally, to prevent the effect of mass transfer on annulus-plane dynamics, a low flow resistant pneumatic check-valve (R-702, Resenex Corp. Chatsworth, CA) was positioned on the ventricular chamber (Fig. 1). The mass of fluid entering from the atrial tube pushed the trapped air in the ventricular chamber to leave the box through the check-valve avoiding the mass transfer effect.

To reproduce the movement of the mitral annulus during early diastole, the valve plane was allowed to freely slide in the downstream end of the atrial tube without friction (Fig. 1). Three L-shaped rods prevented the plate from falling inside the ventricular chamber (Fig. 1). The LV pressure drop was reproduced by a computer-controlled suction pump (Superpump system VSI SPS3891, Vivitro Systems Inc.). The considered range for pressure-drop time constant was within the physiologic range<sup>13,16,61</sup> and the volume of ejected fluid at each cycle was set to 50 mL, which is equivalent to the volume of blood transferred into a normal human LV during early diastole.<sup>24</sup>

Both chambers and the sliding annulus plane were made of Plexiglas to facilitate flow visualization and motion detection of the annulus plane by high-speed cameras. More details about the experimental apparatus can be found in an earlier article.<sup>31</sup>

Carpentier-Edwards' PERIMOUNT™ bioprosthetic heart valves (Edwards Lifesciences, Irvine, CA) in different sizes (21, 23, 25, and 27 mm) were used to mimic the mitral valve function. For each experiment, the appropriate bioprosthetic valve was securely placed within the annulus plane (Fig. 1).

### *Reproduction of Early Diastole*

For each run, both atrial and ventricular chambers were set to start from atmospheric pressure, approximately equal to the physiological pressure in the left atrium prior to rapid filling phase.<sup>24</sup> To reproduce the sudden pressure drop, the suction pump generated a rapid trans-mitral pressure difference. We used four different sizes of heart valves to simulate different flow

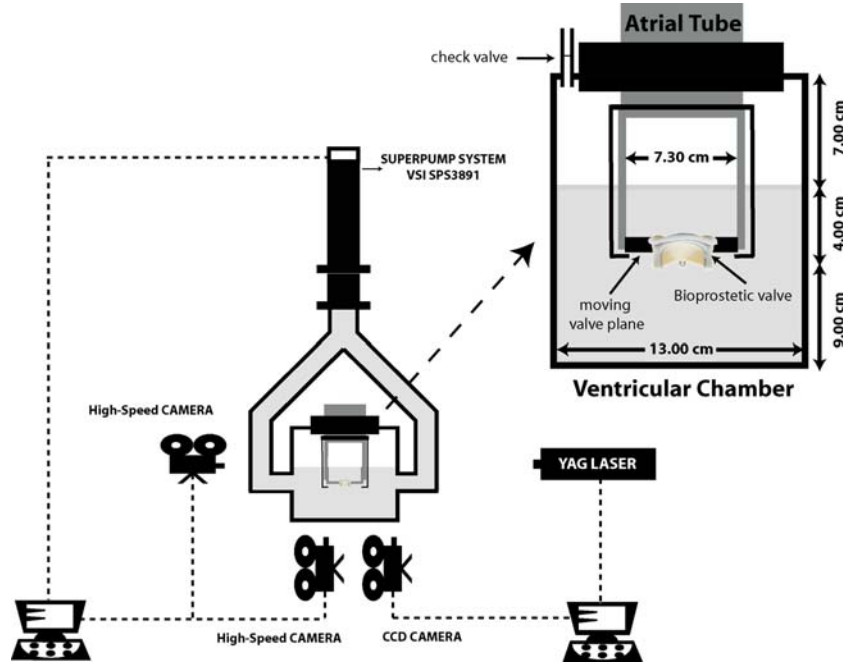


FIGURE 1. Schematics of the experimental setup.

conditions. For all the considered cases, the pump was set to displace a constant volume of fluid (50 mL) while the pressure drop scheme and the initial water height in the system were kept the same. The pressure inside the ventricular chamber was measured by a pressure monitoring system during the experiment (Deltran DPT-400 pressure transducers, Utah Medical Products, Inc, and VSI-TP8891 Vivitro Systems, Inc.).

For accuracy of measurement and to ensure that the obtained results were reproducible and consistent with each other, every set of experiment consisted of 20 consecutive cycles. For each single cycle, the LV pressure was forced to decay as an exponential function in response to the applied suction:

$$P = P_0 \exp\left(\frac{-t}{\tau}\right) \quad (2)$$

where  $t$  was time,  $P_0$  was the initial pressure set to atmospheric value,  $\tau$  were the pressure-drop time constants and adjusted to  $35 \pm 5$  and  $20 \pm 5$  ms. The duration of each cycle was set to  $100 \text{ ms}^{8,9,19}$  imitating the duration of rapid filling phase of diastole (E wave).

#### Measurement Methods

The displacement of water level inside the atrial tube, displacement of annulus plane, and the opening area of the valve were measured with three synchronized high-speed cameras (Photron FASTCAM-Ultima, PHOTRON USA, Inc. San Diego, CA) at 250 frames per second (fps). The water level velocity was computed by finite difference based on measured

water-level data. Applying continuity and considering a uniform profile for exit jet velocity over the valve cross-section, trans-mitral flow rate was computed as:

$$\frac{dV}{dt} = A(U_A(t) - U_V(t)) = S(t)(U_J(t) - U_V(t)) \quad (3)$$

where  $dV$  is the volume element of fluid going through the valve,  $U_J(t)$  is the magnitude of trans-mitral instant exit jet velocity (Fig. 2),  $U_A(t)$  is the instant magnitude of water-level velocity at the atrium (Fig. 2),  $U_V(t)$  is the instant magnitude of valve plane velocity (Fig. 2),  $S(t)$  is the instant open cross-section area of the valve measured from images captured by a high-speed camera (Photron FASTCAM-Ultima), and  $A$  is the constant cross sectional area of atrial chamber (Table 1). Instantaneous exit jet velocity ( $U_J$ ) was computed from (3) as:

$$U_J = \frac{A}{S} U_A + \left(1 - \frac{A}{S}\right) U_V \quad (4)$$

The movement of annulus plane monitored by a high-speed camera (Photron FASTCAM-Ultima) was synchronized with the water level velocity and valve's opening area. Mass of the fluid inside the atrial tube at each instant of time was computed as:

$$\rho \int_{V_0}^{V_A(t)} dV_A = \rho \left( V_0 - \frac{\pi}{4} D_A^2 \left( x_0 - \int_{x_0}^{x(t)} dx \right) \right) \quad (5)$$

where  $\rho$  is water density,  $dV_A$  is the fluid volume element,  $V_0$  is the initial volume of the fluid inside the atrium,  $x_0$  is the initial position of atrial water level

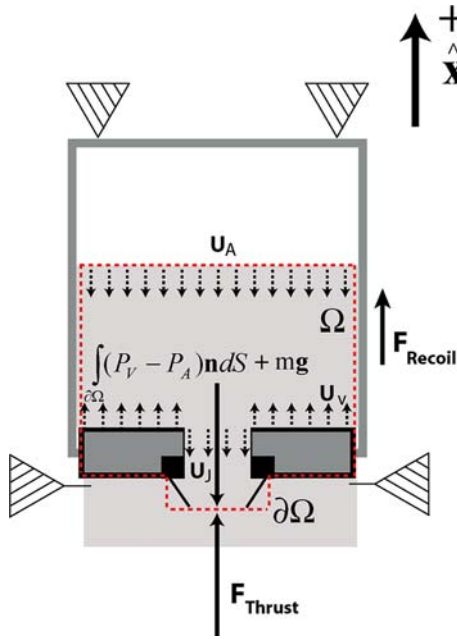


**FIGURE 2.** Embedded control volume ( $\Omega$ ) of fluid inside the atrial tube and at the trans-mitral position. Broken line shows the embedded control volume. Black broken arrows show the velocity vectors.  $U_J$  is the instantaneous trans-mitral jet velocity vector,  $U_V$  is the valve plane velocity vector, and  $U_A$  is the water-level velocity vector at the atrium. The negative sign indicates the opposite direction of vectors with respect to the reference positive direction. Forces are shown with long solid vectors. Recoil force is the resultant of thrust and the pressure forces. The positive direction is shown on the figure.

**TABLE 1.** Abbreviations and acronyms.

|                      |   |
|----------------------|---|
| $P$                  | Pressure at nozzle                          |
| $P_0$                | Initial pressure at ventricle               |
| $\tau$               | Pressure-drop time constant                 |
| $V$                  | Volume of fluid passes the valve            |
| $U_J$                | Instantaneous exit jet velocity             |
| $U_A$                | Water-level velocity at the atrium          |
| $U_V$                | Valve (annulus) plane velocity              |
| $D_J$                | Diameter of the jet                         |
| $D_A$                | Atrial tube diameter                        |
| $\rho$               | Water density                               |
| $V_A$                | Instantaneous volume of fluid in atrium     |
| $V_0$                | Initial volume of fluid in atrium           |
| $X_0$                | Initial position of water level in atrium   |
| $X$                  | Instantaneous position of water-level       |
| $T^*$                | Formation time                              |
| $t$                  | Time  |
| $M$                  | Mass of the annulus plane plus atrial fluid |
| $G$                  | Gravitational acceleration                  |
| $a_V$                | Valve (annulus) plane acceleration          |
| $M_{\text{Annulus}}$ | Mass of the annulus plane                   |
| $P_A$                | Pressure at atrial tube                     |
| $P_V$                | Pressure at the tip of the valve            |

with respect to the laboratory coordinate system prior starting the experiment,  $x(t)$  is the instant position of water level, and  $dx$  is the atrial water level displacement element. Vortex formation time ( $T^*$ ) for tempo-

rally variable nozzle<sup>12</sup> was computed from the modified equation as:

$$T^* = \int_0^t \frac{U_J(\zeta) - U_V(\zeta)}{D_S(\zeta)} d\zeta \quad (6)$$

where  $(U_J - U_V)$  is the magnitude of relative instantaneous exit jet velocity,  $D_S$  is the effective open valve diameter, and  $t$  is the time.

### Flow Visualization and Measurement

The flow characteristic information (e.g., velocity and vorticity fields) were captured by phase-averaged Digital Particle Image Velocimetry (DPIV).<sup>60</sup> DPIV uses two digital images of a particle-seeded flow illuminated by a thin laser sheet to determine the displacement field of the particles in the field of view (sampling window) by cross-correlating pixels in a subsection of two images. Flow was seeded with neutrally buoyant, orange fluorescent particles with the diameter in the range of 60–80  $\mu\text{m}$ . A high-resolution monochrome CCD digital camera (30 fps, 768  $\times$  480; TM-9701, PULNiX America, Inc.) was positioned perpendicular to the ventricular chamber to capture the image sequences of the particle seeded flow field (Fig. 1). The pair of images were captured from illuminated sheet of fluorescent particles generated by a 25 mJ double pulsed Nd:YAG laser (Gemini, New Wave Research, Inc., Fremont, CA) with the pulse separation of 1 ms.

The duration of each pressure-drop cycle was set to 100 ms, as mentioned earlier. The CCD camera took two pairs of images in each cycle. There were 20 consecutive cycles which were identical due to the same applied pressure drop ( $\tau = 35 \pm 5$  or  $\tau = 20 \pm 5$ ). The obtained DPIV data were phase-averaged over the 20 identical cycles. Therefore, a total of 40 velocity/vorticity fields were captured for all time-points of the rapid-filling phase. This temporal resolution gave us an accurate estimate of the velocity and the vorticity fields to compute circulation<sup>30</sup> of the vortex ring and to validate the exit jet velocity ( $U_J$ ) obtained from a different experimental method (4). The CCD camera was triggered simultaneously by the first cycle of the experiment and was synchronized with the Photron high-speed cameras. The laser sheet was set perpendicular to the trans-mitral jet and cut through the center of the mitral valve annulus. This configuration allowed analysis of velocity and vorticity resulting from the starting jet at the illuminated cross-section.

### Control Volume Analysis

The momentum equation related to the setup was derived by considering the control volume ( $\Omega$ ) equations for the fluid inside the atrial tube and at trans-mitral area



(Fig. 2). No-slip boundary condition was considered adjacent to the atrial tube walls and adjacent to the opening (or fully open) leaflets. Therefore, the water level velocity vector ( $\mathbf{U}_A$ ) at the top and the relative jet velocity vector at the nozzle ( $\mathbf{U}_J + \mathbf{U}_V$ ) are the only non-zero velocity vectors at the control volume's boundaries (Fig. 2). Flow was considered inertia dominant because the Reynolds number for peak trans-mitral flow was greater than 6000 at the tip of the valve. Therefore, shear stress contribution to the momentum equation was neglected. Assuming constant gravitational field ( $\mathbf{g}$ ) acting on the control volume ( $\Omega$ ) with moving boundary, the momentum equation would be described as:

$$\begin{aligned} \frac{\partial}{\partial t}(m\mathbf{U}_V) + \rho \int_{\partial\Omega} \mathbf{U}_J((\mathbf{U}_J + \mathbf{U}_V)\mathbf{n})ds \\ = m\mathbf{g} + \int_{\partial\Omega} (P_V - P_A)\mathbf{n}ds \end{aligned} \quad (7)$$

where  $\mathbf{U}_J$  is the instant exit jet velocity vector,  $\mathbf{U}_V$  is the annulus plane velocity vector,  $P_V$  is the pressure at the tip of the valve,  $P_A$  is the pressure at the atrial side of the valve (Table 1), and  $m$  is the mass of the annulus plane together with the instant mass of the atrial fluid:

$$m(t) = M_{\text{Annulus}} + \rho \int_{\Omega} dV_A(t) \quad (8)$$

Based on the momentum Eq. (7), mitral annulus recoil is described as

$$\begin{aligned} \mathbf{F}_{\text{recoil}} = \frac{\partial}{\partial t}(m\mathbf{U}_V) = \left( M_{\text{Annulus}} + \rho \int_{\Omega} dV_A \right) \mathbf{a}_V \\ + \left( \rho \frac{\partial}{\partial t} \int_{\Omega} dV_A \right) \mathbf{U}_V \end{aligned} \quad (9)$$

where  $\mathbf{a}_V$  is the mitral valve acceleration vector. Thrust generated by the trans-mitral flow is described from momentum equation as:

$$\mathbf{F}_{\text{thrust}} = \rho \int_{\partial\Omega} \mathbf{U}_J((\mathbf{U}_J + \mathbf{U}_V)\mathbf{n})ds \quad (10)$$

This study considered uniform profile for the flow over the annulus. The only external force that applied to the surface of control volume was the weight of annulus plane in addition to the atrial fluid at each instant of time (7–8).

## RESULTS

### *Trans-mitral Jet Velocity and Formation Time*

The magnitude of trans-mitral jet velocity for each valve was computed based on Eq. (4) and is shown

in Table 2 and Fig. 3. Formation time was computed based on Eq. (6) using the relative instantaneous exit jet velocity and its corresponding effective valve diameter (Table 2). Formation time as a non-dimensional measure of time made the comparison between each experiment possible. Since the size of the valves are different but the ejected volume is constant, the duration of E-wave (early diastole) for each case is different and the best way to compare the measured parameters in temporal order is to plot them as a function of formation time.

Once a physiologic pressure drop was applied ( $\tau = 35 \pm 5$  ms), for  $D = 27$  mm, velocity reached its maximum (93.3 cm/s) at  $T^* = 2.2$  and the trans-annulus flow ended at around  $T^* = 4.1$ . For  $D = 25$  mm, trans-mitral jet reached its peak velocity (120.6 cm/s) at  $T^* = 2.7$  and the flow ended prior to  $T^* = 4.6$ . For  $D = 23$  mm, trans-mitral velocity reached the peak (125.1 cm/s) at  $T^* = 3.0$  and the trans-annulus flow ended at around  $T^* = 5.4$ . Using the smallest mitral valve ( $D = 21$  mm), trans-annulus jet velocity reached its maximum (129.4 cm/s) at  $T^* = 2.6$  and the flow terminated around  $T^* = 6.1$  (Table 2 and Fig. 3a).

By applying a faster pressure drop ( $\tau = 20 \pm 5$  ms), for  $D = 27$  mm, velocity reached its maximal value (89.1 cm/s) at  $T^* = 2.0$  and the trans-annulus flow ended at around  $T^* = 4.3$ . For  $D = 25$  mm, trans-mitral jet reached its peak velocity (123.9 cm/s) at  $T^* = 2.8$  and the flow ended prior to  $T^* = 4.3$ . For  $D = 23$  mm, trans-mitral velocity reached the peak (125.5 cm/s) at  $T^* = 2.8$  and the trans-annulus flow ended at around  $T^* = 5.5$ . For  $D = 21$  mm, trans-annulus jet velocity reached its maximum (147.4 cm/s) at  $T^* = 2.8$  and the flow terminated around  $T^* = 8.2$  (Table 2 and Fig. 3b).

### *Trans-mitral Pressure*

Pressure difference between the atrial tube and ventricular chamber at the annulus ( $P$ ) was measured during pressure drop in each cycle. The trans-mitral pressure normalized with the initial LV pressure ( $P_0$ ) for each case plotted as function of formation time in Fig. 4.

### *Mitral Annulus Velocity*

Mitral annulus velocity for each valve was directly measured from images taken by the high-speed camera as mentioned in the Method section. By applying a physiologic pressure drop ( $\tau = 35 \pm 5$  ms), for  $D = 27$  mm, mitral annulus velocity reached its peak (9.5 cm/s) at  $T^* = 3.6$ . For  $D = 25$  mm, annulus velocity reached its maximal value (9.8 cm/s) at

TABLE 2. Physical dimensions of the bioprosthetic mitral valves used for the experiments.

| Mitral valve size (mm) | Maximum effective opening diameter (cm) | Maximum exit jet velocity (cm/s) |                      | Maximum recoil force (dyne) |                      | $T^*$ for maximum recoil force |                      |
|------------------------|---|----------------------------------|----------------------|-----------------------------|----------------------|--------------------------------|----------------------|
|                        |   | $\tau = 20 \pm 5$ ms             | $\tau = 35 \pm 5$ ms | $\tau = 20 \pm 5$ ms        | $\tau = 35 \pm 5$ ms | $\tau = 20 \pm 5$ ms           | $\tau = 35 \pm 5$ ms |
| 27                     | 2.79                                    | 89.1                             | 93.3                 | 7107                        | 7191                 | 3.30                           | 3.50                 |
| 25                     | 2.27                                    | 123.9                            | 120.6                | 8262                        | 6660                 | 4.10                           | 4.50                 |
| 23                     | 2.11                                    | 125.5                            | 125.1                | 2683                        | 2434                 | 5.30                           | 5.40                 |
| 21                     | 1.98                                    | 147.4                            | 129.4                | 3090                        | 3134                 | 7.80                           | 7.70                 |

Maximum effective opening diameter, magnitude of maximal exit jet velocity, maximal recoil force, and the formation time once the recoil force occurred have been shown.

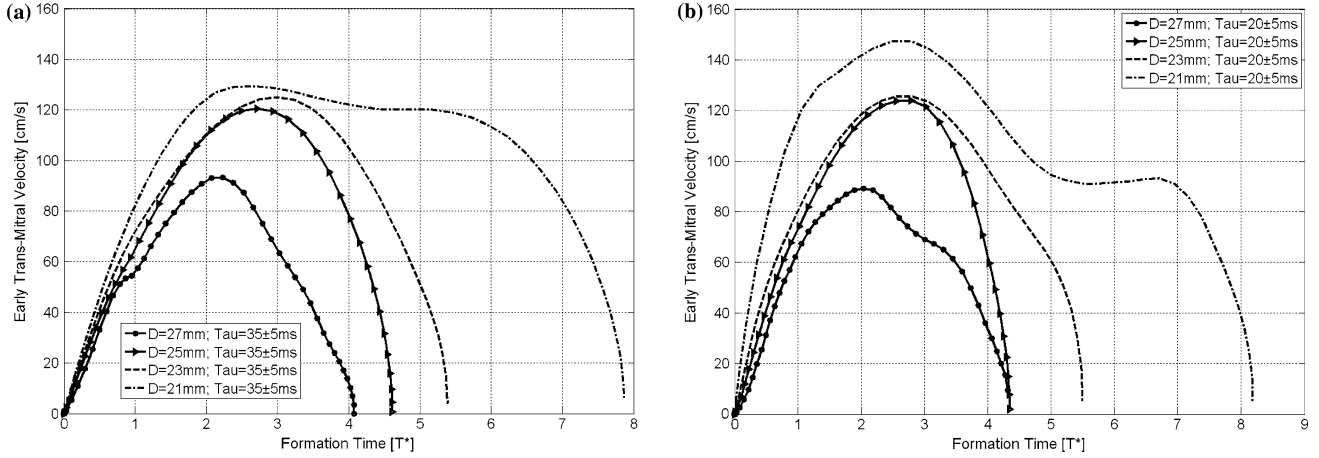


FIGURE 3. Early trans-mitral jet velocity ( $U_J - U_V$ ). (a) Shows trans-mitral jet velocity as function of formation time for different valve sizes due to a pressure drop with the time constant of  $\tau = 35 \pm 5$  ms. (b) Trans-mitral jet velocity as function of formation time for different valve sizes due to a pressure drop with the time constant of  $\tau = 20 \pm 5$  ms.

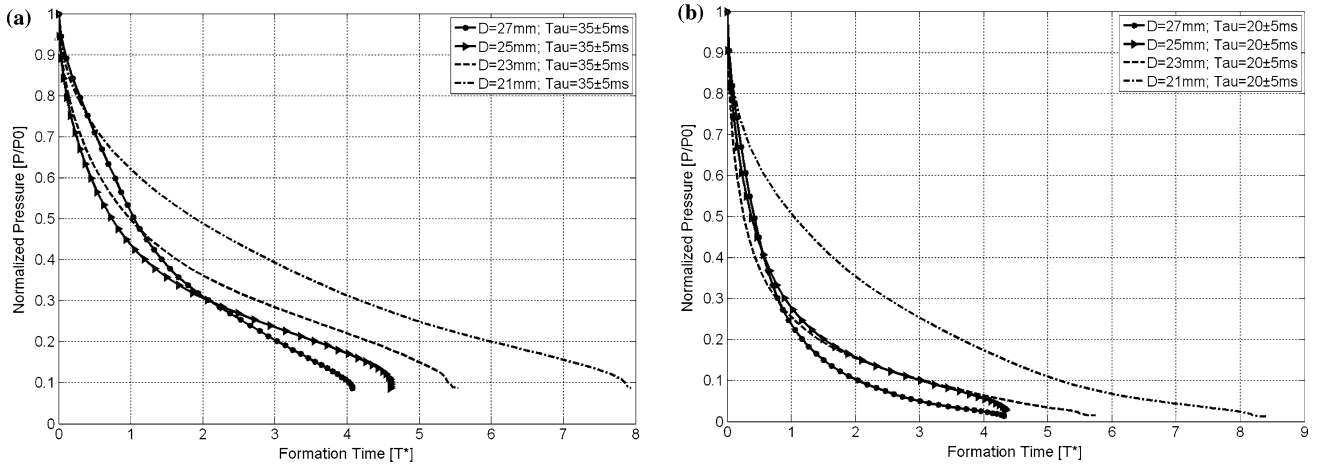
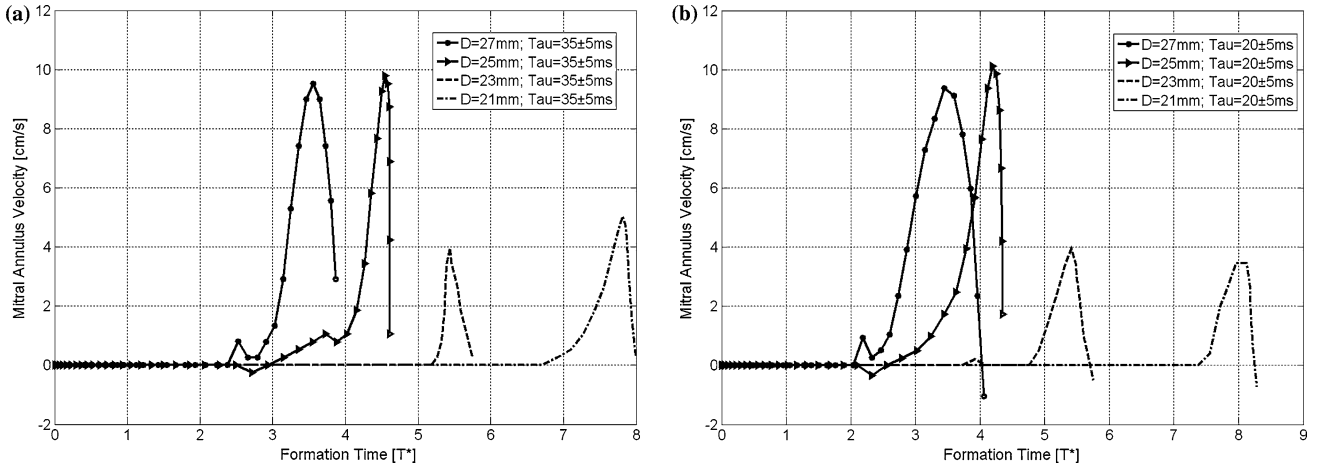


FIGURE 4. Trans-mitral pressure normalized with initial ventricular pressure. (a) Top: shows normalized pressure drop as function of formation time for different valve sizes due to a pressure drop time constant of  $\tau = 35 \pm 5$  ms. (b) Shows normalized pressure drop as function of formation time for different valve sizes due to a pressure drop time constant of  $\tau = 20 \pm 5$  ms.

$T^* = 4.5$ . For  $D = 23$  mm, annulus velocity reached the peak (4.0 cm/s) at  $T^* = 5.4$ . For  $D = 21$  mm, mitral annulus velocity reached its maximum (5.0 cm/s) at  $T^* = 7.8$  (Fig. 5a).

Applying a faster pressure drop ( $\tau = 20 \pm 5$  ms) resulted in a maximal annulus velocity of 9.4 cm/s at  $T^* = 3.4$  for  $D = 27$  mm. The peak mitral annulus velocity (10.1 cm/s) of the 25 mm valve was attained at



**FIGURE 5.** Mitral annulus velocity ( $E_m$ ). (a) Shows annulus velocity as function of formation time for different valve sizes due to a pressure drop with the time constant of  $\tau = 35 \pm 5$  ms. (b) Annulus velocity as function of formation time for different valve sizes due to a pressure drop with the time constant of  $\tau = 20 \pm 5$  ms.

$T^* = 4.2$ . For  $D = 23$  mm, annulus velocity reached its maximal value (3.9 cm/s) at  $T^* = 5.4$  and for  $D = 21$  mm mitral annulus had its maximal value (3.4 cm/s) at  $T^* = 8.0$  (Fig. 5b).

#### Correlation Between the Valve Size and the Annulus Plane Dynamics

Valve plane acceleration was measured for all the cases and the recoil force was computed from Eq. (9). Recoil force was non-dimensionalized with  $\rho S_{\max} U_{J_{\max}}^2$  for each case; where  $\rho$  is the fluid density,  $S_{\max}$  is the maximum opening of each valve during the trans-mitral flow, and  $U_{J_{\max}}$  is the maximal trans-mitral jet velocity. Figures 6a and 6b compare the effect of pressure drop time-constant on non-dimensional averaged annulus plane recoil as a

function of formation time ( $T^*$ ). The magnitude of peak jet velocity measured for each valve size is also shown in Table 2.

#### Correlation Between the Pressure Drop and the Annulus Plane Dynamics

To study the effect of pressure drop on the annulus recoil, two pressure decay programs with different time constants ( $\tau = 35 \pm 5$  ms and  $\tau = 20 \pm 5$  ms) were applied to the atrio-ventricular apparatus. The pressure drop scheme (Fig. 4) followed the same exponential format as mentioned earlier (2). Formation time and the mitral annulus recoil force were computed as stated in Eqs. (3)–(9). Comparative plots of averaged recoil as a function of formation time ( $T^*$ ) for all the valves are depicted in Fig. 7. The negative recoil

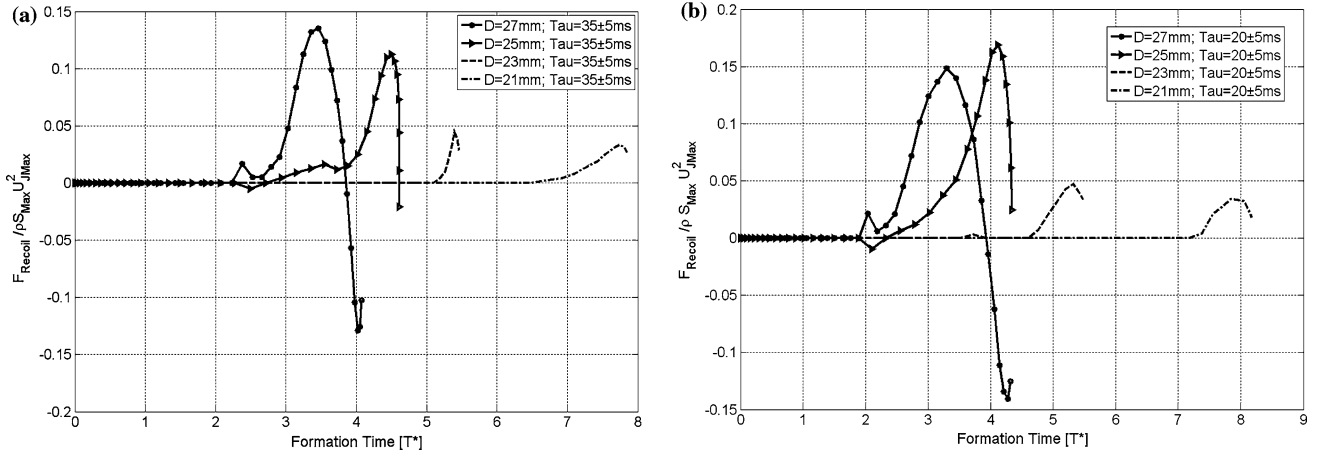


**FIGURE 6.** Averaged normalized annulus recoil force. (a) Shows non-dimensional annulus recoil force as function of formation time for different valve sizes due to a pressure drop with the time constant of  $\tau = 35 \pm 5$  ms. (b) Non-dimensional annulus recoil force as function of formation time for different valve sizes due to a pressure drop with the time constant of  $\tau = 20 \pm 5$  ms.

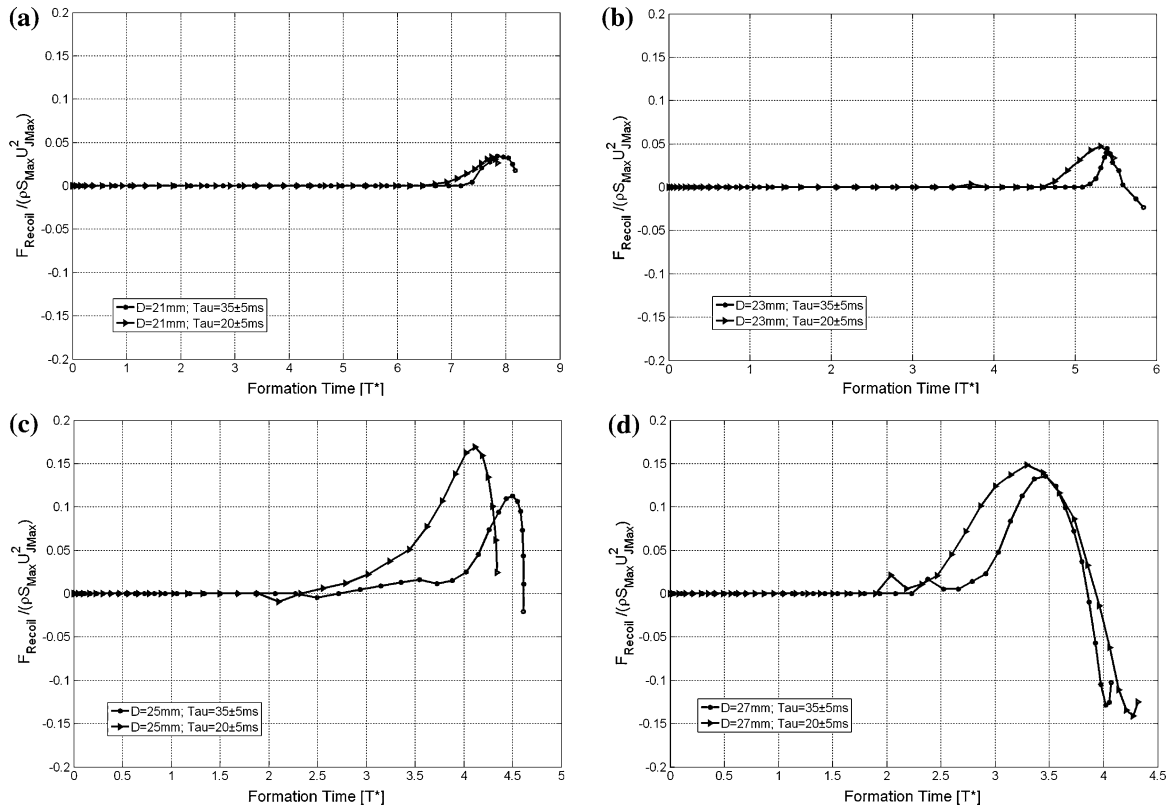


**FIGURE 7.** Comparison of non-dimensional annulus plane recoil force for different pressure drop programs ( $\tau = 35 \pm 5$  ms versus  $\tau = 20 \pm 5$  ms). (a)  $D = 21$  mm; (b)  $D = 23$  mm; (c)  $D = 25$  mm; and (d)  $D = 27$  mm.

represents the change in direction of the recoil force applied to the annulus once the valve reaches its maximal distance from the original position of the plane (sitting on the L-shaped bars).

For the valve size 21 mm, variation in pressure-drop time constant did not induce a significant change in the magnitude or at the onset of the maximal recoil (Table 2 and Fig. 7a). Variation of pressure-drop time-constant using a 23 mm mitral valve resulted in a change in magnitude of recoil force (Table 2), but no significant change at the peak incident (Table 2 and Fig. 7b). However, both magnitude and incident of the peak recoil remarkably changed in response to a pressure drop variation once a 25 mm valve were positioned at mitral place (Table 2 and Fig. 7c). For the 27 mm valve, change in pressure drop time-constant resulted in a delay at the non-dimensional incident of the recoil peak while the magnitude of the peak did not change considerably (Table 2 and Fig. 7d).

#### *Correlation Between Vortex Formation and the Annulus Plane Dynamics*

The vorticity field for each case was obtained from DPIV measurements during trans-mitral flow.

Figures 8 and 9 depict the vorticity fields captured simultaneously with the peak annulus recoil due to the LV pressure drop.

Figure 8 shows the vorticity field captured at the maximal recoil force after applying a pressure drop with the time constant of  $\tau = 35 \pm 5$  ms. Figures 8a and 8b depict the vorticity field for valve sizes 21 mm and 23 mm, respectively, superimposed over its corresponding particle-seeded flow field once the recoil reached its maximal value. The vorticity fields shown in both subfigures demonstrate the leading vortex ring has pinched off from its generating jet and a significant trailing jet has appeared. Figure 8c shows the vorticity contour plot immediately after completion of the pinch-off process from a 25 mm valve. Figure 8d shows an isolated vortex ring ejected from a 27 mm valve. As it appears, the vortex ring has not yet pinched off from its generating jet.

Vorticity field obtained concurrent with the peak recoil followed by applying a faster pressure drop ( $\tau = 20 \pm 5$  ms) are shown in Fig. 9. The pinched off leading vortex ring and a considerable trailing jet is captured for the valve sizes 21 mm and 23 mm (Figs. 9a and 9b, respectively). Figure 9c shows a newly pinched-off vortex ring from a 25 mm valve. The vortex ring appears to be in an earlier formation



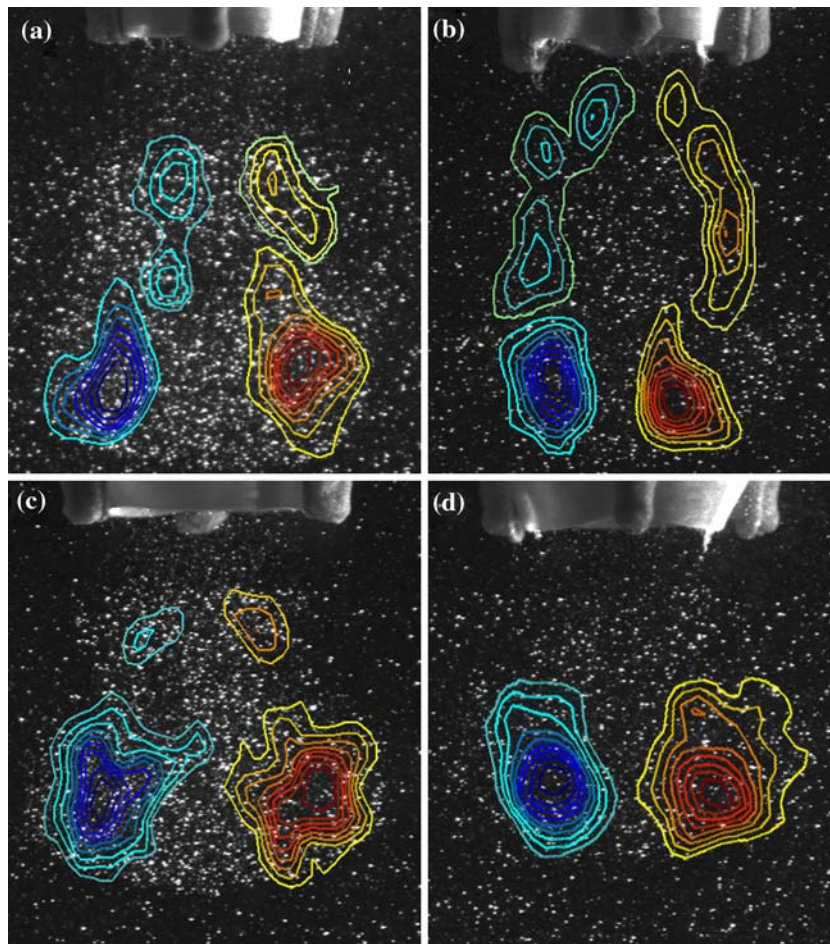


**FIGURE 8.** Vorticity contour plots computed from DPIV measurements during trans-mitral flow for each valve size when pressure decay time constant is assigned to  $\tau = 35 \pm 5$  ms. (a)  $D = 21$  mm; (b)  $D = 23$  mm; (c)  $D = 25$  mm; and (d)  $D = 27$  mm.

stage than in Fig. 8c. Figure 9d shows a growing vortex ring ejected from a 27 mm valve.

## DISCUSSION

The general motivation for this study was to assess the pure effects of atrio-ventricular flow field on the mitral valve dynamics. Based on previous studies, it has been shown that the variation in trans-mitral flow would be reflected in diastolic motion of the mitral annulus.<sup>41</sup> Moreover, the fact that the LV acts as a suction pump during diastole has been confirmed by a number of earlier studies.<sup>6,27,37</sup> Performance of this suction pump depends on several parameters such as chamber compliance, atrio-ventricular pressure gradient, operation and the size of the mitral valve, and the proper propagation of the contraction waves which makes the comprehensive ventricular assessment tricky. On the other hand, diastolic dysfunction is a pathological condition that regardless of its origin,

eventually gives rise to a mechanically dysfunctional suction pump incapable of receiving adequate volume of blood during filling phases. As a result, quantitative assessment of the trans-mitral jet and mitral valve dynamics which are strongly correlated with the performance of the suction pump can lead us to a more accurate evaluation of LV during diastole.

The critical role of vortex ring formation rests on the relative contribution of the leading vortex ring and the trailing jet (which appears after pinch-off) to the thrust supplied to the flow.<sup>39</sup> In a recent paper,<sup>31</sup> we measured the average recoil exerted on an annulus plane during rapid filling phase as a function of formation time (1), and showed that it would be maximal when the formation time reaches around the value of 4. This condition was achieved only by implementing physiologic values for the annulus diameter (without leaflets) and LV pressure drop to experimentally model the rapid filling phase. However, kinematics of the heart valve's leaflets as they open and close during diastole seem to interact with the process of vortex ring

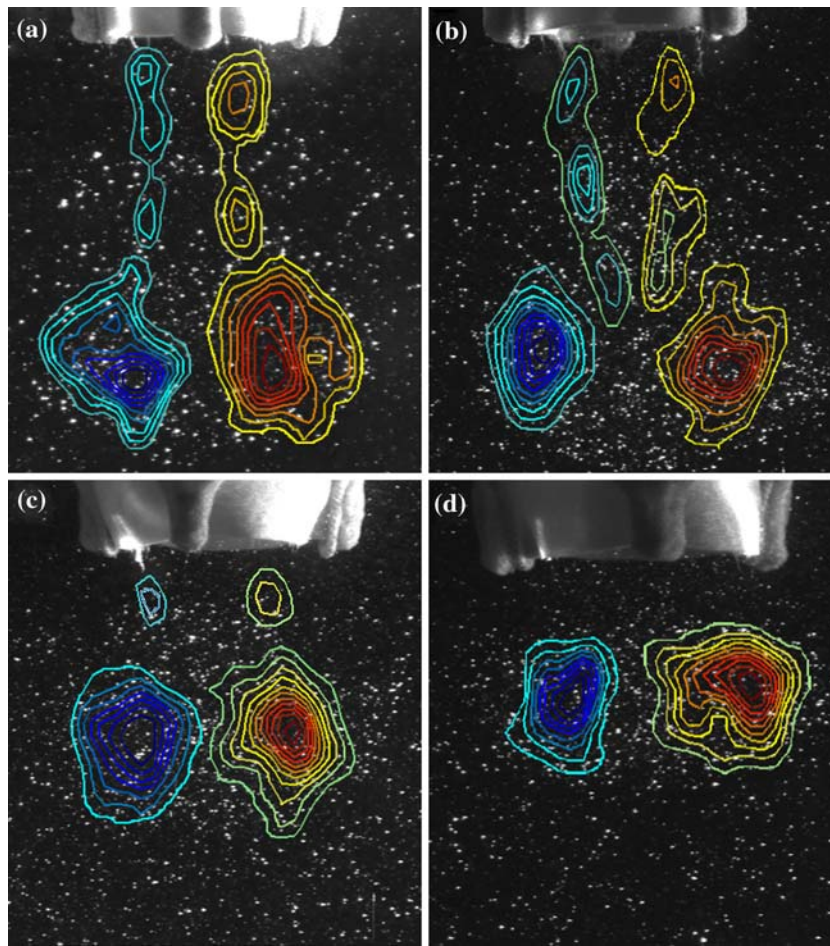


**FIGURE 9.** Vorticity contour plots computed from DPIV measurements during trans-mitral flow for each valve size when pressure decay time constant is assigned to  $\tau = 20 \pm 5$  ms. (a)  $D = 21$  mm; (b)  $D = 23$  mm; (c)  $D = 25$  mm; and (d)  $D = 27$  mm.

formation, thus complicating the response of the mitral annulus to the pressure drop. In the present work, we considered the interaction of trans-mitral jet with the leaflets.

In an intact heart, motion of the mitral annulus during the rapid filling phase represents the recoil force applied to the base of the heart. This motion is the consequence of interrelated changes in several parameters including LV volume status,<sup>11</sup> left atrial pressure,<sup>40</sup> atrioventricular flow,<sup>51</sup> mitral annulus shape,<sup>28,50</sup> and the rate of myocardial relaxation.<sup>1</sup> All these factors can also affect the LV flow structure. In the present study, we recapitulated the involved factors within the index of vortex formation time to quantify the mitral annulus recoil force based on that. We followed the process of vortex ring formation due to the LV pressure drop—as a sign of myocardial relaxation—in different flow conditions. We also substitute the myocardial relaxation effect with the LV pressure drop; bioprosthetic valves were used in mitral position and the left atrial pressure and the

ejected volume were chosen similar to physiologic state.

Comparing the status of the forming vortex ring with the non-dimensional instant of maximum recoil in case of  $\tau = 35 \pm 5$  ms (Fig. 8), it can be observed that for valve sizes 21 mm and 23 mm, the ring has pinched off before the recoil reaches its peak value, denoting that the momentum has been mostly transferred through the remaining trailing jets. However, in mitral valves with larger diameter, the vorticity field (Fig. 8) indicates that the vortex ring is still forming ( $D = 27$  mm) or the ring has just pinched off ( $D = 25$  mm) at the time the maximal recoil is achieved. Considering the magnitude of the recoil force, it can be observed that the maximal recoil, as well as the maximal annulus velocity, is generated over the valve once the vortex ring pinches off. By increasing the rate of pressure drop ( $\tau = 20 \pm 5$ ), the peak recoil occurred at an earlier formation time for larger valve diameters (25 mm and 27 mm) and the magnitude of the peak has also changed (Fig. 6b). On

the basis of the vorticity contour plots for different pressure drop cases (Figs. 8c, 8d, 9c, and 9d), it can be inferred that the non-dimensional recoil would be maximal once the vortex ring is about to pinch off, regardless of the valve size or the pressure-drop time constant. This is also true for the mitral annulus velocity which is correlated with the recoil.

By placing smaller valves (21 mm and 23 mm) in mitral position, the magnitude of the recoil did not show any significant change once the rate of the pressure drop increased (Figs. 7a and 7b). The explanation for this phenomenon lies within the fact that in these cases, the momentum is mostly transferred by trailing jets rather than the vortex ring. Since the final size of the vortex ring is relatively small, its contribution to the momentum transfer is less than the trailing jet, and therefore, the onset of vortex ring pinch off does not affect the magnitude of annulus velocity and the recoil force, respectively.

Plotting the magnitude of peak recoil versus formation time for all the studied cases (Fig. 10) show that the recoil is maximal when occurs at the formation time ranging from 3.5 to 4.5. This range is congruent with the optimum range of formation time previously reported in the literature.<sup>17,18,31,39</sup>

In this study, we confirm that the recoil generated by pulsatile trans-mitral jet is a significant contributing factor in mitral annulus dynamics and annulus velocity, respectively. Other conditions such as altered LV geometry, impaired relaxation and/or viscose deformations can also affect the mitral annulus recoil by affecting the trans-mitral pressure gradient. It should also be noted that the parameters such as compliance

effect and mitral valve saddle shape are also responsible for annulus dynamics which we did not consider them in this study.

#### *The Role of Leaflets in Dissipation of the Annulus Plane Recoil*

In an earlier study,<sup>31</sup> we used a similar experimental setup to replicate the diastolic rapid filling phase due to an exponential pressure drop ( $\tau = 35 \pm 5$  ms), by means of an annulus without leaflets. The recoil force ( $F_{\text{recoil}}$ ) was computed based on momentum equation for three different sizes of annulus (17.5 mm, 25 mm, and 30 mm). The recoil force was correlated with the vortex formation, implying that the maximal recoil achieved when the vortex ring was pinched off.

In the present study, we found that the magnitude of mitral annulus recoil is remarkably lower than the magnitude of recoil in an annulus without leaflets, even if the same pressure drop scheme is applied. In Fig. 10, the recoil force is linearly regressed to formation time, and its magnitude is compared in three different cases of no-leaflet ( $\tau = 35 \pm 5$  ms), with leaflet ( $\tau = 35 \pm 5$  ms), and with leaflet ( $\tau = 20 \pm 5$  ms). This reduction in magnitude of recoil force is particularly evident in the case of  $D = 25$  mm which exists in all three groups of experiment (Fig. 10). The formation time range at which the maximal recoil occurred did not change considerably with respect to existence of the leaflets.

Considering the remarkable lower recoil force in presence of leaflets, it can be concluded that the existence of leaflets would dissipate the recoil force. This

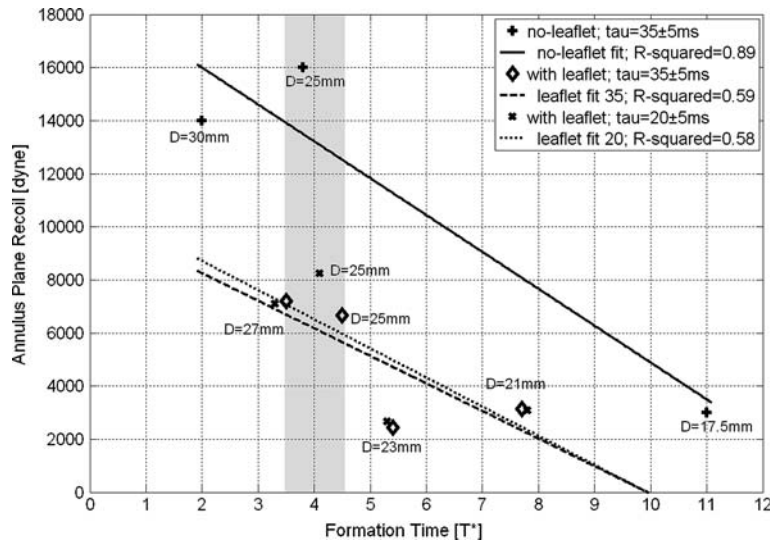


**FIGURE 10.** Maximal recoil force magnitude versus formation time. The gray band shows the range of formation time that the maximal magnitude of recoil force has occurred at, in each set of experiment. “+” is related to no-leaflet experiment from previous study; “♦” is related to recoil for annulus with leaflets when the pressure scheme has a  $\tau = 35 \pm 5$  ms, and “\*” is related to recoil for annulus with leaflets when the pressure scheme has a  $\tau = 20 \pm 5$  ms. Goodness of the fits are shown by  $R$ -squared.



damping effect might be explained by the birth of three-dimensionality in the jet resulted from changes in orifice eccentricity because of presence of the leaflets. Based on the results of a numerical simulation, Bolzon *et al.*<sup>5</sup> suggested that finite changes in orifice eccentricity would generate a fully three-dimensional vortex wake that evolves quite differently from the one developed under an axisymmetric condition. Based on their theory, the resulted diastolic vortex ring deviates from quasi-axisymmetric geometry due to the leaflet interaction, and in fact, deforms progressively due to self-induced motion. Accordingly, there would be viscous reconnection of the wake vortex lines that are adjacent to the wall with the boundary layer vortex lines as the early phase of wake dissipation.

It should also be mentioned that most patients with early diastolic failure still have the native bicuspid mitral valve as opposed to the bioprosthesis and hence the shape of the valve and the leaflet geometry might have a significant influence on the nature of the vortical flow particularly with regard to the stability of the vortex ring and the damping effect.

#### *Validation of the Results with In Vivo Measurements*

Given that the non-invasive measurement of mitral annulus recoil is difficult, the clinical approach for assessment of mitral annulus dynamics is to measure the peak annulus velocity by Doppler tissue imaging (DTI). The mean peak early diastolic mitral annulus velocity in normal cases has been reported as  $10.0 \pm 1.3$ ,<sup>51</sup>  $13.0 \pm 1.6$ ,<sup>54</sup> and  $11.0 \pm 2.6$  cm/s<sup>59</sup> in independent studies. The same velocity has been shown being progressively declined in pseudonormal/restrictive groups ( $5.3 \pm 1.2$ ,<sup>51</sup>  $6.6 \pm 1.9$ ,<sup>54</sup> and  $8.9 \pm 3.5$  cm/s<sup>59</sup>) measured by clinicians. In our *in vitro* study, the magnitude of peak mitral annulus velocity for larger valves ( $D = 27$  mm and  $D = 25$  mm) was  $10.23 \pm 1.16$  cm/s, and for smaller valves ( $D = 23$  mm and  $D = 21$  mm) was  $4.10 \pm 0.66$  cm/s (Fig. 5). The resulted numbers are comparable with the clinically measured velocities.

The reason that the annulus velocity (Fig. 5), in average, is higher in 25 mm and 27 mm valves than 21 mm and 23 mm valves is the correlation of the annulus velocity with the mitral valve recoil force. Therefore, the magnitude of the mitral annulus velocity would be maximal in the same manner the recoil force maximizes once the vortex ring is about to pinch off, regardless of the valve size or the pressure-drop time constant. The explanation for lower annulus velocity in 23 mm and 21 mm lies within the fact that in these cases, the momentum is mostly transferred by trailing jets rather than the vortex ring. Since the final size of the vortex ring is relatively small, its contribu-

tion to the momentum transfer is less than the trailing jet, and therefore, the onset of vortex ring pinch-off does not affect the magnitude of annulus velocity and the recoil force.

The trans-mitral pressure drop during isovolumic relaxation phase followed by early LV filling in a normal left ventricle is an exponential curve which results in a faster pressure drop at the beginning (isovolumic relaxation) and a slower drop while the mitral valve is open and the ventricular volume is increasing.<sup>29,55</sup> In the present study, the pressure drop exponential functions were set to generate physiologic forms of filling dynamic<sup>55,62</sup> which are comparable with the LV function (Figs. 3 and 4). This type of pressure drop resulted in opening the valve placed in the mitral position and generated an early trans-mitral flow similar to an E-wave. The normal range of trans-mitral jet velocity (E-wave) measured by ultrasound is  $82 \pm 21$  cm/s.<sup>7,26</sup> The trans-mitral velocity (E-wave) can peak above 120 cm/s in severe diastolic dysfunction (restrictive pattern).<sup>23</sup> In our study, peak trans-mitral velocity for larger diameter valves ( $D = 27$  mm and  $D = 25$  mm) was  $106.7 \pm 18.0$  cm/s, and for smaller valves ( $D = 23$  mm and  $D = 21$  mm) was  $131.8 \pm 10.5$  cm/s, depending on the rate of pressure drop (Table 2). The early trans-mitral velocities for all of the valves are provided in Fig. 3.

## CONCLUSION

The present *in vitro* study confirms the presence of a vortex ring in early diastole and implies that the process of vortex ring formation can influence the mitral annulus dynamics. We also found that mitral valve recoil is maximal once the vortex ring is about to pinch off, regardless of the valve size or the characteristics of ventricular pressure drop. Additionally, interaction of the valve leaflets with the forming vortex ring can dissipate the mitral recoil force. In summary, this study supports the hypothesis that vortex ring formation can be used as an index for assessment of ventricular function during diastole.

## LIMITATIONS

In this study, we did not use a viscous fluid with similar rheological properties as blood. The reason for that was to minimize the effects of viscosity and dissipation on vortex ring formation. Additionally, since the mechanical model we used had different physical properties from myocardium, choosing the conventional blood analogs might not result in a flow condition equivalent to the left heart due to the different

forms of wall–fluid interactions. However, in reality blood viscosity would affect the mitral annulus dynamics and the process of trans-mitral vortex ring formation by increasing the dissipation. The chamber shape we used was different from the shape of the left ventricle. In spite of this, we tried to preserve the base–apex dimensions similar to the left ventricle as well as maintaining the compliance effect by induction of appropriate pressure drop.

In an intact heart, mitral annulus is an integral part of dense tissue covering the mitral valve and parts of the atrial and ventricular chambers. The oval shape and the bi-leaflet structure of the native mitral valve would also affect the stability and the symmetry of the generated vortex ring. However, the extent of the influence of this asymmetry on the process of vortex ring formation has not been investigated here. Moreover, the native mitral annulus is not planar, but instead forms a three-dimensional saddle shape. While we expect that the mitral annulus geometrical shape-change would affect the diastolic vortex ring, this phenomenon was not a focus of the present study. Another limitation of this study was using a phase averaged DPIV technique for flow measurements which slightly increased the error due to the fast nature of the experiments. Works are in progress to use continuous laser for illumination and high-speed cameras for stereo-PIV to obtain more accurate results.

## APPENDIX

### *Clinical Measurement of Formation Time*

Vortex formation time ( $T^*$ ) can be acquired from echocardiography based on non-invasive measurement of the velocity time integral (VTI) resulted from trans-mitral inflow (Fig. A1) during E-wave

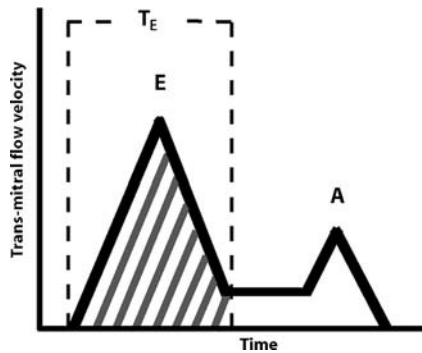


**FIGURE A1.** Schematic of a normal trans-mitral Doppler flow velocity. The area under the E-wave is the time velocity integral (VTI) and reflects the contribution of the rapid filling phase in the LV diastolic filling.  $T_E$  is the duration of E-wave.

( $u_E$ ) and the time-averaged diameter of the mitral valve ( $\bar{D}$ ):

$$T^* = \frac{\int u_E dt}{\bar{D}} \equiv \frac{\bar{U}_E T_E}{\bar{D}}$$

The length of the jet is an equivalent of velocity time integral (area under E-wave) and diameter of the jet is the corresponding diameter of the open mitral valve. Formation time is the ratio of length of the jet over its diameter.

## ACKNOWLEDGMENT

Authors would like to acknowledge Edwards Lifesciences corp. for providing the bioprosthetic heart valves for this study.

## REFERENCES

- <sup>1</sup>Alam, M., and C. Höglund. Assessment by echocardiogram of left ventricular diastolic function in healthy subjects using the atrioventricular plane displacement. *Am. J. Cardiol.* 69:505–565, 1992.
- <sup>2</sup>Appleton, C. P. Doppler assessment of left ventricular diastolic function: the refinements continue. *J. Am. Coll. Cardiol.* 2:1697–1700, 1993.
- <sup>3</sup>Baccani, B., F. Domenichini, G. Pedrizzetti, and G. Tonti. Fluid dynamics of the left ventricular filling in dilated cardiomyopathy. *J. Biomech.* 35(5):665–671, 2002.
- <sup>4</sup>Bellhouse, B. J. Fluid mechanics of a model mitral valve and left ventricle. *Cardiovasc. Res.* 6:199–210, 1972.
- <sup>5</sup>Bolzon, G., L. Zovatto, and G. Pedrizzetti. Birth of three-dimensionality in a pulsed jet through a circular orifice. *J. Fluid Mech.* 493:209–218, 2003.
- <sup>6</sup>Brecher, G. A. Experimental evidence of ventricular diastolic suction. *Circ. Res.* 4:513–518, 1956.
- <sup>7</sup>Bruch, C., A. Schmermund, T. Bartel, J. Schaar, and R. Erbel. Tissue Doppler imaging: a new technique for assessment of pseudonormalization of the mitral inflow pattern. *Echocardiography* 17(6 Pt 1):539–546, 2000.
- <sup>8</sup>Brutsaert, D. L., F. E. Rademakers, and S. U. Sys. Triple control of relaxation: implications in cardiac disease. *Circulation* 69:190–196, 1984.
- <sup>9</sup>Brutsaert, D. L., and S. U. Sys. Relaxation and diastole of the heart. *Physiol. Rev.* 69:1228–1315, 1989.
- <sup>10</sup>Carr-White, G. S., and D. G. Gibson. Mitral annulus dynamics: determinant of left ventricular filling. *J. Cardiol.* 37(suppl 1):27–32, 2001.
- <sup>11</sup>Choong, C. Y., H. C. Herrmann, A. E. Weymann, and M. A. Fifer. Preload dependence of Doppler-derived indexes of left ventricular diastolic function in humans. *J. Am. Coll. Cardiol.* 10:800–808, 1987.
- <sup>12</sup>Dabiri, J. O., and M. Gharib. Starting flow through nozzles with temporally variable exit diameter. *J. Fluid Mech.* 538:111–136, 2005.
- <sup>13</sup>Dong, S. J., P. S. Hees, C. O. Siu, J. L. Weiss, and E. P. Shapiro. MRI assessment of LV relaxation by untwisting rate: a new isovolumic phase measure of tau. *Am. J. Physiol. Heart Circ. Physiol.* 281:H2002–H2009, 2001.



- <sup>14</sup>Fukuda, K., T. Oki, T. Tabata, A. Luchi, and S. Ito. Regional left ventricular wall motion abnormalities in myocardial infarction and mitral annular descent velocities studied with pulsed tissue Doppler imaging. *J. Am. Soc. Echocardiogr.* 11(9):841–848, 1998.
- <sup>15</sup>Galiuto, L., G. Ignone, and A. N. DeMaria. Contraction and relaxation velocities of the normal left ventricle using pulsed-wave tissue Doppler echocardiography. *Am. J. Cardiol.* 81:609–614, 1998.
- <sup>16</sup>Garcia, M. J., N. G. Smedira, N. L. Greenberg, M. Main, M. S. Firstenberg, J. Odabashian, and J. D. Thomas. Color M-mode Doppler flow propagation velocity is a preload insensitive index of left ventricular relaxation: animal and human validation. *J. Am. Coll. Cardiol.* 35:201–208, 2000.
- <sup>17</sup>Gharib, M., E. Rambod, A. Kheradvar, D. Sahn, and J. O. Dabiri. A global index for heart failure based on optimal vortex formation in the left ventricle. *Proc. Natl. Acad. Sci. USA* 103(16):6305–6308, 2006.
- <sup>18</sup>Gharib, M., E. Rambod, and K. Shariff. A universal time scale for vortex ring formation. *J. Fluid Mech.* 360:121–140, 1998.
- <sup>19</sup>Gilbert, J. C., and S. A. Glantz. Determinants of left ventricular filling and of the diastolic pressure/volume-relationship. *Circ. Res.* 64:827–852, 1989.
- <sup>20</sup>Glasson, J. R., G. R. Green, and J. F. Nistal, *et al.* Mitral annular size and shape in sheep with annuloplasty rings. *J. Thorac. Cardiovasc. Surg.* 117:302–309, 1998.
- <sup>21</sup>Glasson, J. R., M. Komeda, and G. T. Daughters, *et al.* Most ovine mitral annular three-dimensional size reduction occurs before ventricular systole and is abolished with ventricular pacing. *Circulation* 96(Suppl II):115–122, 1997.
- <sup>22</sup>Gorman, J. H. III, K. B. Gupta, and J. T. Streicher, *et al.* Dynamic three dimensional imaging of the mitral valve and left ventricle by rapid sonomicrometry array localization. *J. Thorac. Cardiovasc. Surg.* 112:712–726, 1996.
- <sup>23</sup>Groban, L., and S. Y. Dolinski. Transesophageal echocardiographic evaluation of diastolic function. *Chest* 128(5):3652–3663, 2005.
- <sup>24</sup>Guyton, A. C., and J. E. Hall. *Textbook of Medical Physiology*, 10th edn. WB Saunders Company, 2000.
- <sup>25</sup>Hasegawa, H., W. C. Little, M. Ohno, S. Brucks, A. Morimoto, H. J. Cheng, and C. P. Cheng. Diastolic mitral annular velocity during the development of heart failure. *J. Am. Coll. Cardiol.* 41:1590–1597, 2003.
- <sup>26</sup>Hung, M. J., W. J. Cherg, L. T. Kuo, C. H. Wang, and M. S. Chern. Analysis of left atrial volume change rate during left ventricular diastolic phase with M-mode echocardiography for differentiation between normal and pseudonormal mitral inflow. *Am. J. Cardiol.* 89(5):552–556, 2002.
- <sup>27</sup>Ingels, N. B. Jr., G. T. Daughters, S. D. Nikolic, A. De-Anda, M. R. Moon, A. F. Bolger, M. Komeda, G. C. Derby, E. L. Yellin, and D. C. Miller. Left ventricular diastolic suction with zero left atrial pressure in open-chest dogs. *Am. J. Physiol.* 270(4 Pt 2):H1217–1224, 1996.
- <sup>28</sup>Jimenez, J. H., D. D. Soerensen, Z. He, S. He, and A. P. Yoganathan. Effects of a saddle shaped annulus on mitral valve function and chordal force distribution: an in vitro study. *Ann. Biomed. Eng.* 31(10):1171–1181, 2003.
- <sup>29</sup>Kheradvar, A., R. C. Gorman, J. H. Gorman, A. Zeeshan, and M. Gharib. Evaluation of isovolumic relaxation phase in the process of ventricular remodeling following myocardial infarction. *Conf. Proc. IEEE Eng. Med. Biol. Soc.* 5:3654–3657, 2004.
- <sup>30</sup>Kheradvar, A., J. Kasalko, D. Johnson, and M. Gharib. An in-vitro study of changing profile heights in mitral bioprostheses and their influence on flow. *ASAIO J* 52(1):34–38, 2006.
- <sup>31</sup>Kheradvar, A., M. Milano, and M. Gharib. Correlation between vortex ring formation and mitral annulus dynamics during ventricular rapid filling. *ASAIO J* 53(1):8–16, 2007.
- <sup>32</sup>Kheradvar, A., M. Milano, R. C. Gorman, J. H. Gorman III, and M. Gharib. Assessment of left ventricular elastic and viscous components based on ventricular harmonic behavior. *Cardiovasc. Eng.* 6(1):30–39, 2006.
- <sup>33</sup>Kilner, P. J., G. Z. Yang, A. J. Wilkes, R. H. Mohiaddin, D. N. Firmin, and M. H. Yacoub. Asymmetric redirection of flow through the heart. *Nature* 404:759–761, 2000.
- <sup>34</sup>Kim, W. Y., T. Bisgaard, S. L. Nielsen, J. K. Poulsen, E. M. Pedersen, J. M. Hasenkam, and A. P. Yoganathan. Two-dimensional mitral flow velocity profiles in pig models using epicardial echo Doppler Cardiography. *J. Am. Coll. Cardiol.* 24:532–545, 1994.
- <sup>35</sup>Kim, W. Y., P. G. Walker, E. M. Pedersen, J. K. Poulsen, S. Oyre, K. Houlind, and A. P. Yoganathan. Left ventricular blood flow patterns in normal subjects: a quantitative analysis by three dimensional magnetic resonance velocity mapping. *J. Am. Coll. Cardiol.* 26:224–238, 1995.
- <sup>36</sup>Komoda, T., R. Hetzer, and C. Uyama, *et al.* Mitral annular function assessed by 3D imaging for mitral valve surgery. *J. Heart Valve Dis.* 3:483–490, 1994.
- <sup>37</sup>Kovacs, S. J., J. S. Meisner, and E. L. Yellin. Modeling of diastole. *Cardiol. Clin.* 18:459–487, 2000.
- <sup>38</sup>Kranidis, A., K. Kostopoulos, and L. Anthopoulos. Evaluation of left ventricular filling by echocardiographic atrioventricular plane displacement in patients with coronary artery disease. *Int. J. Cardiol.* 48:183–186, 1995.
- <sup>39</sup>Krueger, P. S., and M. Gharib. The significance of vortex ring formation to the impulse and thrust of a starting jet. *Phys. Fluids* 15(5):1271–1281, 2003.
- <sup>40</sup>Kuo, L. C., M. A. Quinones, R. Rokey, M. Sartori, E. G. Abinader, and W. A. Zoghbi. Quantification of atrial contribution to left ventricular filling by pulsed Doppler echocardiography and the effect of age in normal and diseased hearts. *Am. J. Cardiol.* 59:1174–1178, 1987.
- <sup>41</sup>Nagueh, S. F. Noninvasive evaluation of hemodynamics by Doppler echocardiography. *Curr. Opin. Cardiol.* 4:217–224, 1999.
- <sup>42</sup>Nishimura, R. A., and A. J. Tajik. Evaluation of diastolic filling of left ventricle in health and disease: Doppler echocardiography is the clinician's Rosetta stone. *J. Am. Coll. Cardiol.* 30:8–18, 1997.
- <sup>43</sup>Ohno, M., C. P. Cheng, and W. C. Little. Mechanism of altered patterns of left ventricular filling during the development of congestive heart failure. *Circulation* 89:2241–2250, 1994.
- <sup>44</sup>Ommen, S. R., R. A. Nishimura, C. P. Appleton, F. A. Miller, J. K. Oh, M. M. Redfield, and A. J. Tajik. Clinical utility of Doppler echocardiography and tissue Doppler imaging in the estimation of left ventricular filling pressures: a comparative simultaneous Doppler-catheterization study. *Circulation* 102:1788–1794, 2000.
- <sup>45</sup>Ormiston, J. A., P. Shah, C. Tei, and M. Wong. Size and motion of the mitral valve annulus in man. *Circulation* 64:113–120, 1981.
- <sup>46</sup>Pai, R. G., M. Tanimoto, W. Jintapakorn, J. Azevedo, N. G. Pandian, and P. M. Shah. Volume-rendered three-dimensional dynamic anatomy of the mitral annulus using transesophageal echocardiographic technique. *J. Heart Valve Dis.* 4:623–627, 1995.

- <sup>47</sup>Poerner, T. C., B. Goebel, P. Unglaub, T. Sueselbeck, J. M. Strotmann, S. Pflieger, M. Borggreffe, and K. K. Haase. Detection of a pseudonormal mitral inflow pattern: an echocardiographic and tissue Doppler study. *Echocardiography* 20(4):345–356, 2003.
- <sup>48</sup>Reul, H., N. Talukder, and W. Muller. Fluid mechanics of the natural mitral valve. *J. Biomech.* 14:361–372, 1981.
- <sup>49</sup>Rodriguez, F., F. Langer, K. B. Harrington, F. A. Tibayan, M. K. Zasio, A. Cheng, D. Liang, G. T. Daughters, J. W. Covell, J. C. Criscione, N. B. Ingels, and D. C. Miller. Importance of mitral valve second-order chordae for left ventricular geometry, wall thickening mechanics, and global systolic function. *Circulation* 110(11 Suppl 1):III15–122, 2004.
- <sup>50</sup>Salgo, I. S., J. H. Gorman III, R. C. Gorman, B. M. Jackson, F. W. Bowen, T. Plappert, M. G. St John Sutton, and L. H. Edmunds Jr. Effect of annular shape on leaflet curvature in reducing mitral leaflet stress. *Circulation* 106(6):711–717, 2002.
- <sup>51</sup>Sohn, D. W., I. H. Chai, D. J. Lee, and H. C. Kim, *et al.*. Assessment of mitral annulus velocity by Doppler Tissue imaging in the evaluation of left ventricular diastolic function. *J. Am. Coll. Cardiol.* 30:474–480, 1997.
- <sup>52</sup>Standring, S. *Gray's Anatomy: The Anatomical Basis of Clinical Practice*. 39th ed. Edinburgh: Churchill Livingstone, 2004.
- <sup>53</sup>Steen, T., and S. Steen. Filling of a model left ventricle studied by colour M mode Doppler. *Cardiovasc. Res.* 28(12):1821–1827, 1994.
- <sup>54</sup>Su, H. M., T. H. Lin, W. C. Voon, K. T. Lee, C. S. Chu, W. T. Lai, and S. H. Sheu. Differentiation of left ventricular diastolic dysfunction, identification of pseudonormal/restrictive mitral inflow pattern and determination of left ventricular filling pressure by Tei index obtained from tissue Doppler echocardiography. *Echocardiography* 23(4):287–294, 2006.
- <sup>55</sup>Thomas, J. D., and A. E. Weyman. Echocardiographic Doppler evaluation of left ventricular diastolic function: physics and physiology. *Circulation* 84:977–990, 1991.
- <sup>56</sup>Vierendeels, J. A., E. Dick, and P. R. Verdonck. Hydrodynamics of color M-mode Doppler flow wave propagation velocity  $V(p)$ : a computer study. *J. Am. Soc. Echocardiogr.* 15:219–224, 2002.
- <sup>57</sup>Weiss, J. L., J. W. Fredrisen, and M. L. Weisfeldt. Hemodynamic determinants of the time course of fall in canine left ventricular pressure. *J. Clin. Invest.* 58:751–760, 1976.
- <sup>58</sup>Whalley, G. A., H. J. Walsh, G. D. Gamble, and R. N. Doughty. Comparison of different methods for detection of diastolic filling abnormalities. *J. Am. Soc. Echocardiogr.* 18(7):710–717, 2005.
- <sup>59</sup>Wierzbowska-Drabik, K., J. Drozd, M. Plewka, E. Trzos, M. Krzeminska-Pakula, and J. D. Kasprzak. The utility of pulsed tissue Doppler parameters for the diagnosis of advanced left ventricular diastolic dysfunction. *Echocardiography* 23(3):189–196, 2006.
- <sup>60</sup>Willert, C. E., and M. Gharib. Digital particle image velocimetry. *Exp. Fluids* 10(4):181–193, 1991.
- <sup>61</sup>Yamakado, T., E. Takagi, S. Okubo, K. Imanaka-Yoshida, T. Tarumi, M. Nakamura, and T. Nakano. Effects of aging on left ventricular relaxation in humans. *Circulation* 95:917–923, 1997.
- <sup>62</sup>Yellin, E. L., S. Nikolic, and R. W. M. Frater. Left-ventricular filling dynamics and diastolic function. *Prog. Cardiovasc. Dis.* 32(4):247–271, 1990.